

# THE DIURNAL CYCLE OBSERVED BY METEOSAT-8 AND SIMULATED BY A CLIMATE MODEL

Ruth Comer, Anthony Slingo and Richard Allan

ESSC, Reading University

## Abstract

An analysis of the diurnal cycle in clouds and water vapour using observations from Meteosat-8 is presented. A combination of broadband and narrowband data from the GERB (Geostationary Earth Radiation Budget) and SEVIRI (Spinning Enhanced Visible and Infra-Red Imager) instruments provide information about daily variations in surface temperature, cloud and water vapour over Africa and surrounding regions. The high spatial and temporal resolution in the data allow a more detailed analysis than has previously been possible, particularly when considering topographic effects. Outgoing longwave radiation (OLR) data from GERB is analysed using empirical orthogonal functions (EOFs) and reveals interactions between solar heating, surface temperature and cloud evolution. These findings are used to help validate the new HiGEM (High resolution Global Environmental Modelling) high resolution climate model. To extend this work, narrowband radiances from SEVIRI are used to investigate the diurnal cycles in upper tropospheric cloud and humidity.

## INTRODUCTION

The atmospheric diurnal cycle, together with the annual cycle, represents one of the most significant modes of variability. Despite this, the diurnal cycle is well known to be poorly represented in climate models. Many previous studies have used satellite data to investigate the diurnal cycle in clouds and some have used these in validation of models (see Yang and Slingo 2001, for a review). Water vapour is one of the most significant greenhouse gases, but the diurnal cycle in water vapour has received relatively little attention (Soden, 2000).

The current study utilises both broadband and narrowband infra-red data from the Meteosat-8 satellite. The GERB (Geostationary Earth Radiation Budget) instrument is the first to provide broadband outgoing longwave radiation (OLR) from geostationary orbit, giving unprecedented spatial and temporal sampling. Narrowband radiances from SEVIRI (Spinning Enhanced Visible and Infra-Red Imager) are also at higher resolution than have previously been available. Since the atmospheric diurnal cycle is greatest over Africa, Meteosat-8 is ideally located to provide data for this kind of study.

The diurnal cycle in the GERB OLR data is explored using Empirical Orthogonal Function (EOF) analysis to describe the variation in the data. This analysis is repeated for comparison on output from the new HiGEM high resolution climate model. We demonstrate the power of EOFs for separating out physical modes of variation, as well as for comparing two sets of results. The diurnal cycles of upper tropospheric cloud and humidity are compared by applying Soden's (2000) masking method to SEVIRI data. Using a threshold-based cloud mask, signals relating to clouds and water vapour are separated out. Soden's study revealed a two hour time lag between the diurnal cycle of cloud and that of upper tropospheric humidity (UTH). He speculated that this could be due to evaporation of cirrus clouds, but it could be an artefact of the masking method employed.

## DATA & MODEL

The data are from the entire month of July 2004. We use GERB V999 BARG (Binned Averaged Rectified Geolocated) OLR level 2 flux data (see Harries et al. 2005 for data description). This is a pre-release version of the data but changes in the release version should not affect the overall diurnal

cycle results. From SEVIRI we use level 1.5 radiances from the 10.8  $\mu\text{m}$  window channel and the 6.2  $\mu\text{m}$  water vapour channel. Where SEVIRI images are missing for any particular time, a linear interpolation is used. Since there are several missing images from 28 July 2004, this day is discounted from the SEVIRI averaging.

HiGEM (High resolution Global Environmental Model) is a high resolution version of the latest Hadley Centre climate model. It is currently being developed by a consortium led by the Centre for Global Atmospheric Modelling, Reading University, UK. This analysis uses output from an atmosphere only model run, forced by July 1979 sea surface temperatures. The run uses a 20 minute time-step, N144 spatial resolution (approximately 100km) and 38 layers. Radiation calls are made every time-step to provide the broadband OLR.

## METHOD

The GERB and HiGEM results are processed using Empirical Orthogonal Function (EOF) analysis. To facilitate a direct comparison with GERB, the HiGEM output is restricted to a disk over Africa. EOFs and principal components (PCs) are calculated to describe respectively spatial and temporal variation in the data. The first PC describes the dominant signal, having maximum possible temporal variation. Each subsequent PC describes the maximum variation of the data set after that of the preceding PCs has been removed. Each PC has a corresponding EOF, which shows where in the disk the variation associated with that PC is significant.

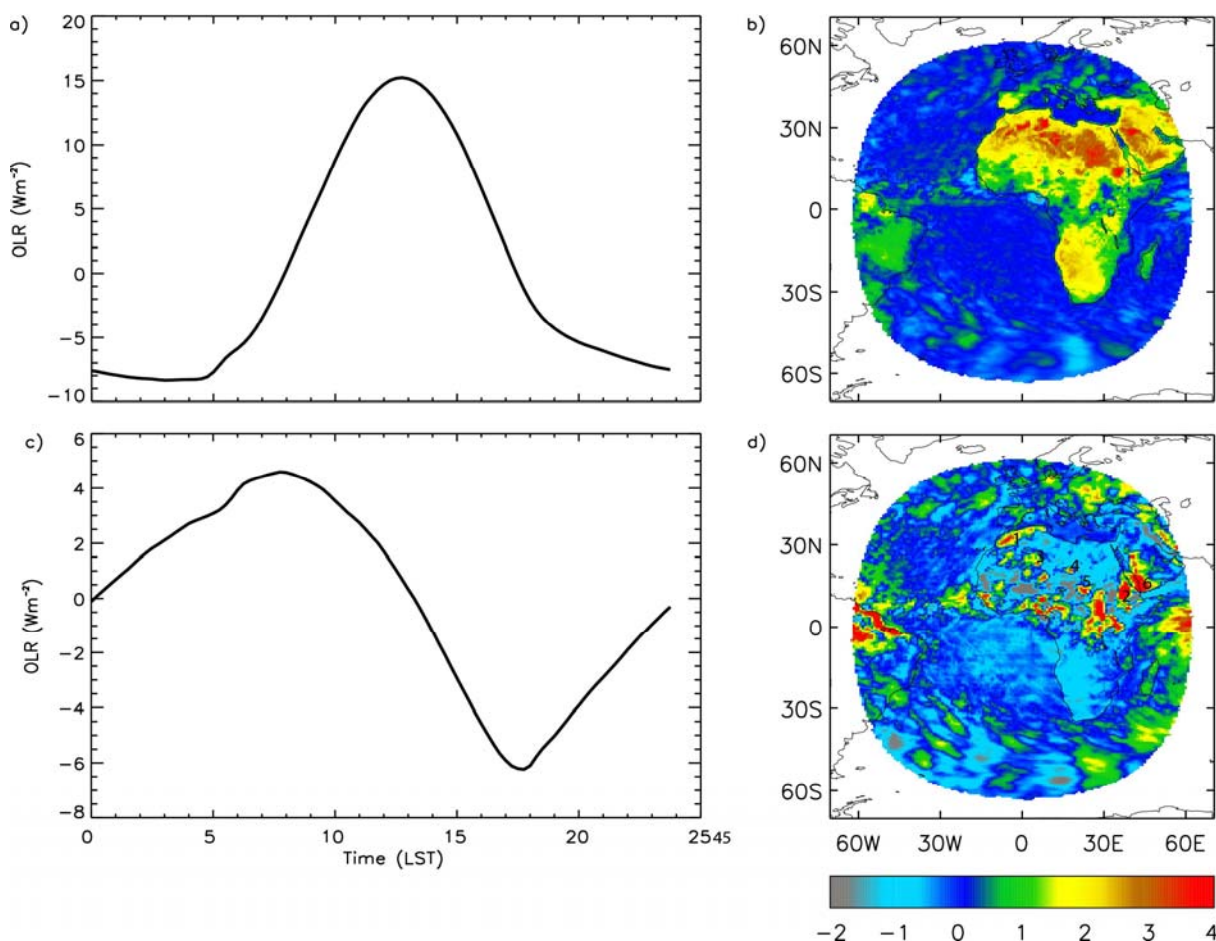


**Figure 1:** First two principal components for GERB data (a,c) together with their respective empirical orthogonal functions (b,d)

The PCs and EOFs are computed following the method described by Smith and Rutan (2003). Separate monthly means are calculated for each fifteen minute slot and the data interpolated to local

solar time (LST). This averaged local time diurnal cycle is arranged into a matrix. The covariance matrix is then calculated, the eigenvectors of which are the PCs. The EOFs are found by applying the diurnal cycle matrix to each PC vector.

Information about upper tropospheric humidity (UTH) comes from SEVIRI's 6.2 $\mu$ m water vapour channel. To investigate the diurnal cycle in UTH, as many cloudy pixels as possible must be removed from the data sample. This is done, following Soden's method, by comparing the brightness temperature of the 6.2 $\mu$ m water vapour channel ( $T_b^{6.2}$ ) with that of the 10.8 $\mu$ m window channel ( $T_b^{10.8}$ ). Since the window channel is relatively insensitive to changes in UTH, the 10.8 $\mu$ m  $T_b$  is significantly warmer than the 6.2 $\mu$ m  $T_b$  for pixels without upper tropospheric cloud. We therefore only use pixels where  $T_b^{10.8} - T_b^{6.2} > 25\text{K}$ . Soden (2000) described this threshold as "somewhat arbitrary", but pointed out that reasonable changes in the threshold did not significantly affect the results. The diurnal cycle in the water vapour channel brightness temperature is calculated for each pixel by averaging the non-masked data for each time of day. The frequency that the cloud mask is applied provides an estimate of upper tropospheric cloud cover.

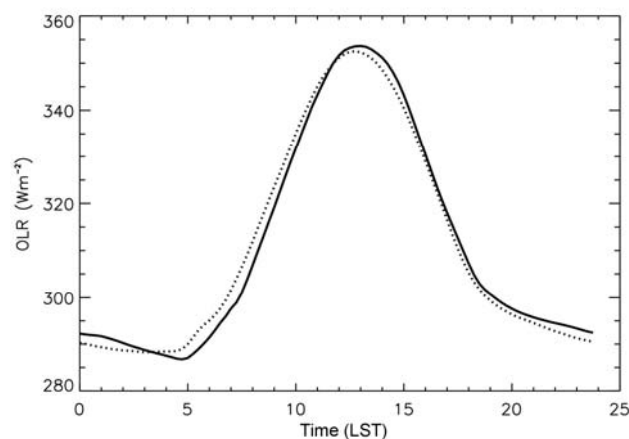


**Figure 2:** Comparison of mean diurnal cycle in GERB data over sahara (solid) with contribution from first principal component (broken)

## RESULTS

Figure 1 shows the first two principal components (PCs) for the averaged GERB OLR diurnal cycle, together with their respective empirical orthogonal functions (EOFs). The first PC (Fig. 1a) accounts for 77.6% of the overall variation in the data. The shape of the curve displays a distinctive surface temperature response to solar heating, increasing from dawn and peaking an hour after local noon. Since this surface heating has its highest extent over the desert regions, these have the highest values in the first EOF (Fig. 1b). Figure 2 further illustrates this significance, showing that the mean diurnal cycle over the Sahara is nearly identical to the contribution from the first PC.

The second PC (Fig. 1c) describes a modification in the OLR data for cloud variation. This PC explains 12.8% of the variation in the data, so we have 90.4% described by just the first two. The positive signals in EOF2 relate to convective cloud over land. The cloud is triggered by the surface heating (represented by the first PC) just after dawn and as it grows to a maximum extent at about 1700-1800 LST the OLR is forced to decrease as the cloud tops grow to higher, colder levels. Many of the largest convective cloud signals in the GERB view are associated with topographical features. Visible in EOF2 are the Atlas Mountains [1], the Ethiopian highlands [2], the Hoggar [3], Tibesti [4] and Marra plateau [5], the Yemeni highlands [6] and several other smaller mountain ranges.

Also visible in EOF2 is a positive banded structure over north-east Brazil. The coastal band is a convective system, probably formed by the interaction of land-sea breezes with the mean easterly flow (Kousky, 1980). The system propagates inland and is reactivated the following evening to form the second band (Garreaud and Wallace, 1997; Cohen et al., 1995). Negative signals over the ocean in

EOF2 correspond to low-level stratocumulus cloud. This reaches its maximum extent just before dawn and is dissipated over the day by solar heating (Dai, 2001).

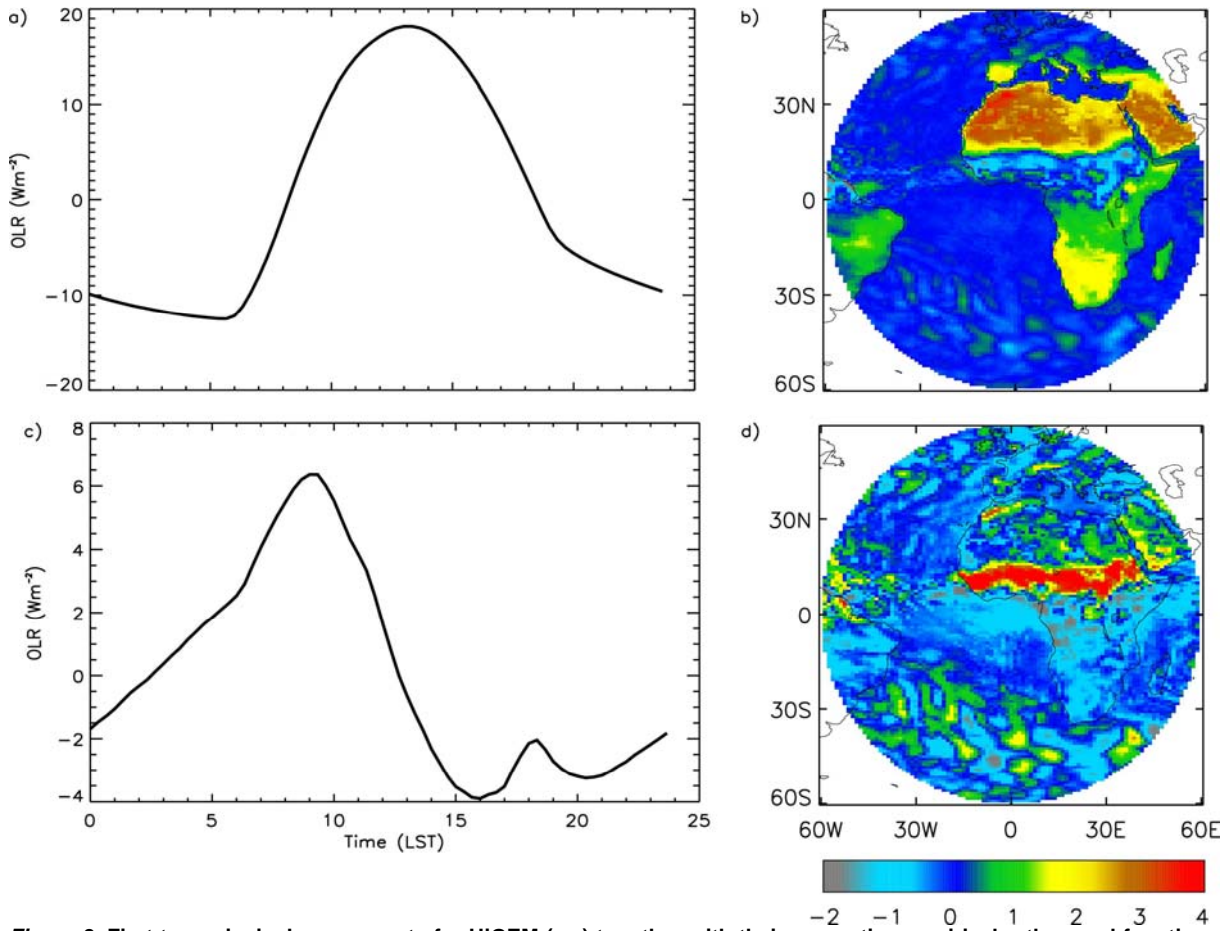


Figure 3: First two principal components for HiGEM (a,c) together with their respective empirical orthogonal functions (b,d)

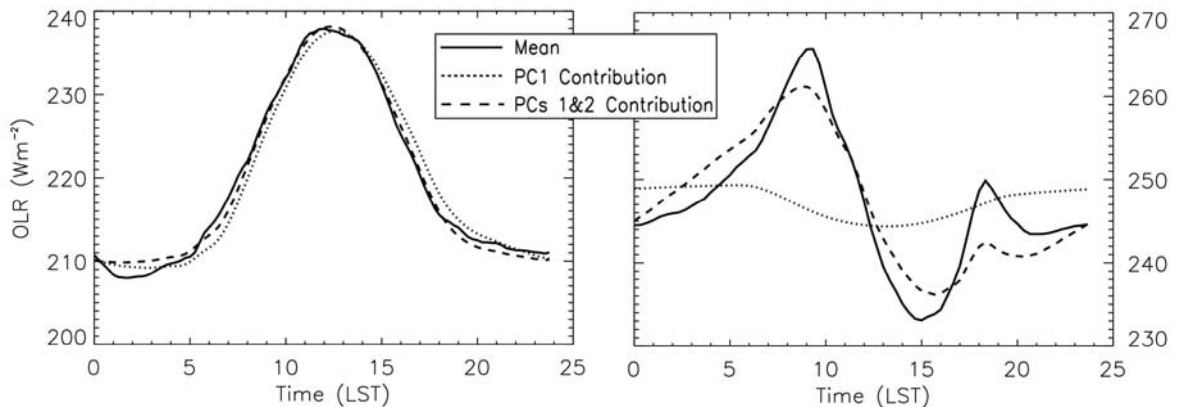
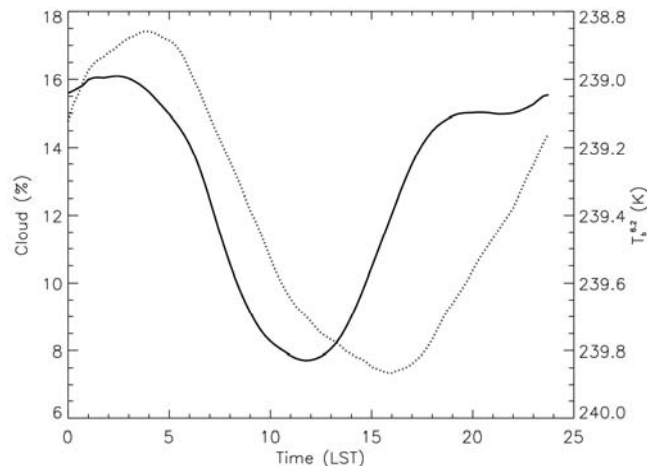


Figure 4: Comparison of ITCZ region for GERB (left) and HiGEM (right) showing mean diurnal cycles and contributions from principal components

For comparison to these GERB results, the first two PCs and EOFs for the HiGEM output are shown in Figure 3. The first principal component (Fig. 3a c.f. GERB, Fig. 1a) shows that the model represents the surface response to solar heating quite well, with the OLR increasing from dawn, and peaking around 1300 LST. The first EOF (Fig. 3b) shows that the largest OLR variations are over the deserts, as in the observations. Both EOFs show large signals in the ITCZ which do not correspond to anything visible in the satellite data. This problem is probably caused by the model's convection being

initiated too readily and too early. Figure 4 illustrates the differences over the ITCZ. The mean curve and contributions from the first two PCs for GERB are shown on the left, and the same for HiGEM on the right. The mean curve (solid) for HiGEM follows the familiar surface heating pattern until around 0900 LST. It then plummets, reaching a minimum at 1500 LST and rises back to join what would be a cooling curve at 1800 LST. This supports the idea that the convection, too early and too extensive, is damaging the signal. The contribution from the first PC for HiGEM (dotted line) is negative since here the cloud signal is more significant than the surface heating signal.



**Figure 5:** Mean diurnal cycle for upper tropospheric cloud (solid) and cloud-cleared  $T_b^{6.2}$  (broken) for West Africa study area

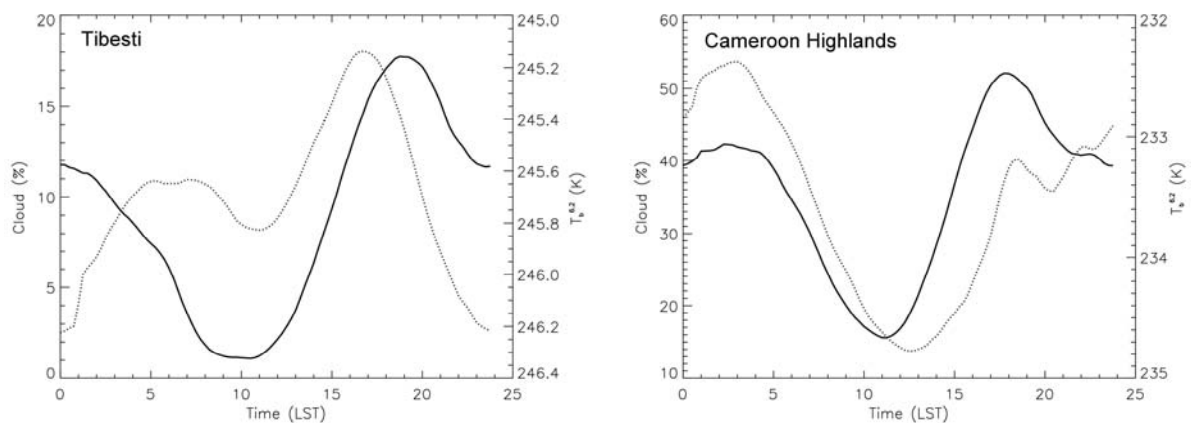


**Figure 6:** Mean diurnal cycle for upper tropospheric cloud (solid) and cloud-cleared  $T_b^{6.2}$  (broken) for Tibesti and Cameroon Highlands

The second EOF (Fig. 3d) outside the ITCZ captures the convective cloud signals. The model reproduces the effect of topography for initiation of convection, since the Atlas Mountains and Yemeni Highlands show high signals in EOF2. The banded structure over Brazil noted above is also visible for HiGEM. The second principal component (Fig. 3c) is slightly distorted around 1800 LST. This is because the unusual signal in the ITCZ is large enough to affect the whole EOF analysis. The analysis was repeated with the ITCZ region masked out (not shown) and the second principal component became much closer to that of GERB.

Figure 5 shows the average diurnal cycles in upper tropospheric cloud and cloud-cleared water vapour channel brightness temperature ( $T_b^{6.2}$ ) over a region of West Africa, roughly 12W-26E, 0-27N. Note that the scale for cleared  $T_b^{6.2}$  has been reversed so that maximums in cloud and UTH can be more easily compared. The diurnal cycle in cleared  $T_b^{6.2}$  shows a minimum (and hence maxima of UTH) one to two hours after the cloud begins to dissipate. This agrees with the findings of Soden (2000) over central America. Taking averages over smaller areas, however, we see that the simple picture breaks down. Figure 6 shows the average diurnal cycles over the Tibesti mountain and Cameroon

Highlands. Here the maximum in UTH appears to precede the maximum in cloud. This could be due to the general uplift in upper tropospheric water vapour in the convective process. A more detailed analysis is required to investigate this further. In particular, the easterly advection which is prevalent over this part of Africa may affect the static time-mean analysis.

## CONCLUSIONS & FUTURE WORK

The new GERB instrument on Meteosat-8 has proved valuable for studying the physical processes involved in the diurnal cycle of cloud over Africa and surrounding regions. The high resolution and position of the instrument make it ideal for exploring the daily variation. Empirical Orthogonal Function Analysis separates the variation neatly into surface temperature and cloud variations, as well as proving a powerful tool for comparing two sets of results. It is possible to isolate problems to particular regions (in this case the ITCZ) simply by comparing one or two EOF plots. With the exception of the ITCZ region, the HiGEM model performs well at representing surface heating and convective cloud, including the significance of topography and the propagating systems over Brazil.

This work is now being extended to explore the diurnal cycle in upper tropospheric humidity (UTH) using 6.2  $\mu\text{m}$  water vapour channel radiances from SEVIRI. The initial results indicate that there is an overall two-hour time lag between upper tropospheric cloud and humidity in West Africa, as found over central America by Soden (2000). The work will now focus on a more localised study to explore specific cloud events, particularly in convective regions. This will include tracking the upper tropospheric cloud, using the threshold mask and a simple maximum overlap method (e.g. Williams and Houze, 1987).

The RADAGAST (Radiative Atmospheric Divergence using ARM Mobile Facility, GERB and AMMA Stations) project brings together data from satellites with ground-based radiative measurements from the ARM (Atmospheric Radiation Measurement) Mobile Facility, currently based in Niger. This will provide a useful resource for a localised case study, exploring how the diurnal cycle in radiative fluxes at the surface relates to that at the top of the atmosphere. These surface measurements can be used to help validate the perceived atmospheric diurnal cycle processes in the analysis of Meteosat-8 data.

## REFERENCES

- Cohen, J., M. S. Dias, and C. Nobre (1995), Environmental conditions associated with Amazonian squall lines: A case study, *Mon. Weather Rev.*, **123**, 3163–3174.
- Dai, A. (2001), Global precipitation and thunderstorm frequencies. Part II: Diurnal variations, *J. Climate*, **14**, 1112–1128.
- Harries, J., and Coauthors (2005), The Geostationary Earth Radiation Budget (GERB) project, *Bull. Amer. Meteorol. Soc.*, **86**, 945–960.
- Kousky, V. (1980), Diurnal rainfall variation in northeast Brazil, *Mon. Weather Rev.*, **108**, 488–498.
- Garreaud, R., and J. Wallace (1997), The diurnal march of convective cloudiness over the Americas, *Mon. Weather Rev.*, **125**, 3157–3171.
- Soden, B.J. (2000), The diurnal cycle of convection, clouds, and water vapor in the tropical upper troposphere. *Geophys. Res. Lett.* **27**, 15 pp 2173-2176.
- Smith, G., and D. Rutan (2003), The diurnal cycle of outgoing longwave radiation from Earth Radiation Budget Experiment measurements, *J. Atmos. Sci.*, **60**, 1529–1542.
- Williams, M., and R. Houze (1987), Satellite-Observed Characteristics of Winter Monsoon Cloud Clusters, *Mon. Weather Rev.*, **115**, 505-519.
- Yang, G.-Y., and J. Slingo (2001), The diurnal cycle in the tropics, *Mon. Weather Rev.*, **129**, 784–801.